

Microstructural and Phase Composition Differences Across the Interfaces in Al/Ti/Al Explosively Welded Clads



DAGMARA MALGORZATA FRONCZEK, ROBERT CHULIST,
LIDIA LITYNSKA-DOBRZYNSKA, GABRIEL ALEJANDRO LOPEZ,
ANNA WIERZBICKA-MIERNIK, NORBERT SCHELL, ZYGMUNT SZULC,
and JOANNA WOJEWODA-BUDKA

The microstructure and phase composition of Al/Ti/Al interfaces with respect to their localization were investigated. An aluminum-flyer plate exhibited finer grains located close to the upper interface than those present within the aluminum-base plate. The same tendency, but with a higher number of twins, was observed for titanium. Good quality bonding with a wavy shape and four intermetallic phases, namely, $TiAl_3$, $TiAl$, $TiAl_2$, and Ti_3Al , was only obtained at the interface closer to the explosive material. The other interface was planar with three intermetallic compounds, excluding the metastable $TiAl_2$ phase. As a result of a 100-hour annealing at 903 K (630 °C), an Al/TiAl₃/Ti/TiAl₃/Al sandwich was manufactured, formed with single crystalline Al layers. A substantial difference between the intermetallic layer thicknesses was measured, with 235.3 and 167.4 μm obtained for the layers corresponding to the upper and lower interfaces, respectively. An examination by transmission electron microscopy of a thin foil taken from the interface area after a 1-hour annealing at 825 K (552 °C) showed a mixture of randomly located $TiAl_3$ grains within the aluminum. Finally, the hardness results were correlated with the microstructural changes across the samples.

DOI: 10.1007/s11661-017-4169-8

© The Author(s) 2017. This article is an open access publication

I. INTRODUCTION

AMONG the high-energy rate forming methods that use the energy from an explosion, three main techniques can be distinguished: powder compaction, explosive forming, and explosive welding (EXW).^[1] These methods are economically beneficial and allow nanostructured materials to be obtained, for example, consolidated samples from nanometric copper powders,^[2] Ni/NiAl metal-matrix composites containing up

to 57 vol pct NiAl particulate,^[3] new shapes of materials,^[4,5] and integrally bonded composites.^[6-9] These advantages make the methods suitable for a large number of technological applications.^[1]

Many of the studies presented in the literature are focused specifically on the EXW process. As confirmed by various attempts, the joining of flat surfaces^[6-9] or tubes^[10-12] can be easily performed by this method. Furthermore, the process can be carried out both under water^[13-16] and under air atmospheres.^[6-11,17,18] This method is steadily increasing its potential applications and improving the obtained results. As a first example, the works completed by Gulenc *et al.*^[19] in producing wire-reinforced multilayer composites are discussed. In this case, EXW was used to join two commercially pure aluminum plates with a steel mesh in-between, and the final product showed better mechanical properties than conventional aluminum clads. According to the authors, these composites have applications in the space and automobile sectors, as well as for other structural applications.^[19,20] For alloys, detailed studies on an explosively welded bilayered CuCrZr alloy/316LN-IG steel performed by Wang *et al.*^[21] proved that this material, for applications in harsh environments, successfully qualified as an enhanced heat flux first wall of

DAGMARA MALGORZATA FRONCZEK, ROBERT CHULIST, LIDIA LITYNSKA-DOBRZYNSKA, ANNA WIERZBICKA-MIERNIK, and JOANNA WOJEWODA-BUDKA are with the Institute of Metallurgy and Materials Science Polish Academy of Sciences, 25 Reymonta Street, 30-059 Kraków, Poland. Contact emails: d.fronczek@imim.pl; dfronczek@gmail.com GABRIEL ALEJANDRO LOPEZ is with the Departamento de Física Aplicada II, Facultad de Ciencia y Tecnología, Universidad del País Vasco, Apdo. 644, 48080 Bilbao, Vizcaya, Spain. NORBERT SCHELL is with the Institute of Materials Research, Helmholtz-Zentrum Geesthacht, Max-Planck-Strasse 1, 21502 Geesthacht, Germany. ZYGMUNT SZULC is with the High Energy Technologies Works 'Explomet', 100H Oswiecimska Street, 45-641 Opole, Poland.

Manuscript submitted December 7, 2016.

Article published online June 28, 2017

the International Thermonuclear Experimental Reactor component. Another impressive example is the production of Al/Ti clads, which were successfully obtained with not only 2^[22] or 3^[23] layers, but 21^[24] or even 40 layers.^[25] The EXW technique can also be used in the production of multilayered materials with significantly different properties, for example, metallic-intermetallic laminate composites. These composites belong to a new class of materials, whose properties combine the large ductility of the metal matrix and the high hardness of intermetallic phases.^[26] Such versatile materials are used in the production of electrical wires and industrial machinery (Al/Cu),^[7,27] platters in the aerospace (Al/Ti)^[24] and automobile (Al/Mg)^[28] industries, and composites for medical applications (Ti/Al₂O₃/NiCr).^[29]

Generally, the EXW process can be divided into three basic stages: detonation of an explosive material; deformation and acceleration of the flyer plate; and, finally, collision of the clads.^[1] The EXW process used to join aluminum and titanium clads leads to the occurrence of several Al-Ti intermetallic phases. Alternatively, further annealing causes the growth of a thermodynamically favored TiAl₃ intermetallic phase.^[23,25,30–33]

The manufacturing of EXW clads requires a number of parameters to be controlled, such as the collision angle, impact velocity, detonation pressure, and geometry, with respect to the type of bonded materials.^[28,34–39] However, the problem becomes even more complicated when more than only one interface is obtained. Therefore, in this manuscript, the simplest case with only two interfaces obtained in three-layered Al/Ti/Al clads is discussed. Significant changes in the microstructure and phase composition of both interfaces are presented. The influence of interface localization with respect to the explosive material and the neighboring regions is also studied.

II. MATERIALS AND METHODS

Two cold-rolled plates of A1050 (further referred to as Al) (150 mm × 240 mm × 1 mm) and one of Ti Gr. 2 (further referred to as Ti) (150 mm × 240 mm × 0.8 mm) were explosively welded in a parallel system under an air atmosphere by the Explomet Company, as schematized in Figure 1(a). A thin layer of silicon was placed on top of the aluminum plate to prevent erosion. The detonation velocity was about 1900 to 1950 m/s. From the state obtained directly after welding, a three-layered material was cut into pieces from the central part in order to obtain samples of 6 mm × 12 mm × 2.8 mm in size (Figure 1(b)). One part of the samples was annealed at 903 K (630 °C) for 100 hours in a vacuum. Subsequently, abrasive papers and diamond polishing pastes mixed with alumina were used to obtain mirror-finished cross sections.

The surface observations were carried out using scanning electron microscopy (SEM), with an FEI Quanta 3D field emission gun (FEG) equipped with a

Trident energy-dispersive X-ray spectrometer (EDS) produced by EDAX* and a TSL electron backscatter

*EDAX is the global leader in Energy Dispersive X-ray Spectroscopy, Electron Backscatter Diffraction, Wavelength Dispersive X-ray Spectrometry and X-ray Fluorescence systems. EDAX Inc., 91 McKee Drive, Mahwah, NJ.

diffraction (EBSD) system, a PHILIPS XL30 equipped with a LINK ISIS EDS system (Oxford Instruments)**,

**Oxford Instruments is a leading provider of high technology tools and systems for research and industry. We design and manufacture equipment that can fabricate, analyse and manipulate matter at the atomic and molecular level. Oxford Instruments, Tubney Woods Abingdon, Oxfordshire, Great Britain.

and a JEOL[†] JSM 7000F. To obtain a proper surface

[†]JEOL is a trademark of Japan Electron Optics Ltd., Tokyo.

quality for the EBSD measurements, the following equipment and parameters were used for the electrolytic etching: a Struers[‡] electropolishing LectroPol-5

[‡]Struers is the world's leading materialographic solution supplier. Struers ApS, Pederstrupvej, 84 Ballerup, Denmark.

machine, a Struers electrolyte A3, an electrolyte temperature of 283 K (10 °C), a voltage of 35 V, a specimen temperature of 77 K (−196 °C), a polishing time of 15 seconds, and a flow rate of 15.

The structural information for the intermetallic phases present at particular interfaces was investigated using high-energy synchrotron radiation (87.1 keV, $\lambda = 0.014235$ nm) and the P07 beamline at DESY[§] in

[§]DESY (Deutsches Elektronen-Synchrotron) is one of the world's leading accelerator centres. Notkestr. 85 Hamburg, Germany.

Hamburg. In order to ensure that the signal coming from only one of the interfaces was collected, the samples were ground either from the upper or lower side into smaller pieces (red dashed lines in Figure 1(b)).

Electron transparent thin foils for transmission electron microscopy (TEM) were cut from the properly selected regions of the bonds using a FEI Quanta 3D Dualbeam focused ion beam. Details of the microstructure were revealed using a FEI TECNAI G2 FEG super TWIN (200 kV) microscope equipped with a Phoenix EDS, also manufactured by EDAX.

Differential scanning calorimetry (DSC) was applied in conjunction with TEM to investigate the effect of a high-temperature treatment on the thin foils. The

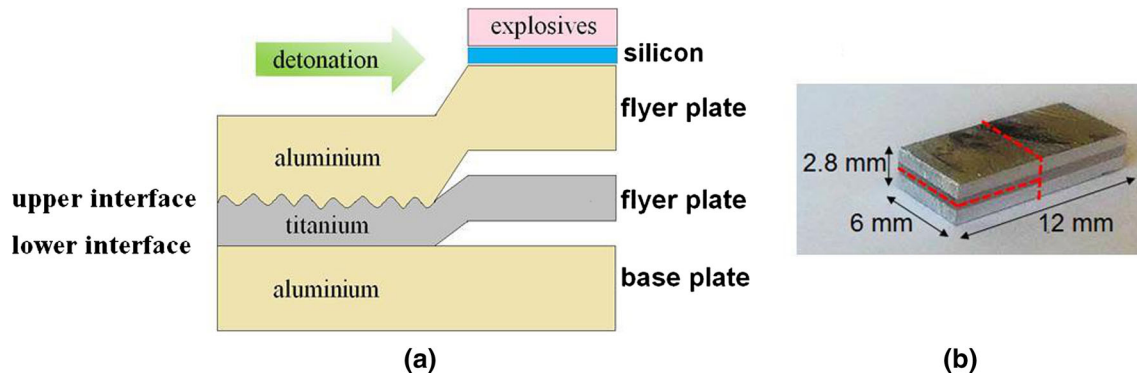


Fig. 1—(a) Schematic setup of the explosively welded Al/Ti/Al system and (b) a photograph of the sample used in experiments.

DSC analyses were performed in a DSC 404 F1 Pegasus, NETZSCH^{§§}. During DSC measurements,

^{§§}The NETZSCH Group consists of three Business Units under the umbrella of the Erich NETZSCH GmbH & Co. Holding KG. The Analyzing & Testing business unit of the NETZSCH Group develops and manufactures a complete high-precision instrument line for thermal analysis and thermophysical properties measurement, as well as offering world class commercial testing services in their laboratories. Erich NETZSCH GmbH & Co. Holding KG, Gebrüder-Netzsch-Straße 19, Selb, Germany.

the samples were placed in aluminum crucibles and protected against oxidation with flowing argon. After heating at a rate of 20 K (20 °C)/min, the samples were annealed at 825 K (552 °C) for 1 hour.

Finally, Vickers hardness measurements were carried out on polished samples using a microhardness tester from CSM[¶] Instruments at room temperature. A sharp

[¶]Anton Paar TriTec SA develops, manufactures and sells instruments to characterize mechanical properties of surfaces. The company has been a global leader in this market for more than 30 years, first under the name of LSRH, CSEM and then CSM Instruments SA. Anton Paar GmbH has acquired CSM Instruments SA in November 15, 2013. Anton Paar TriTec SA Rue de la gare, 4 Peseux, Switzerland.

needle tip with a load of 0.09807 N was used for all indentations. The force was maintained for a dwell time of 15 seconds. The obtained results were averaged from at least five indentation measurements.

III. RESULTS AND DISCUSSION

A. Microstructure

A typical interface obtained in the state directly after EXW is presented in Figure 2. Depending on the welding conditions, *i.e.*, collision angle and distance from the detonation point, different interface morphologies were obtained. In the case of the interface located closer to the explosive material (upper interface), a wavy mode was achieved (Figure 2(a)). The average values of the amplitude were determined to be between 5 and 20 μm , with a varied wavelength of 20 to 350 μm . A

similar tendency in wave parameters (various wavelengths) was reported by Mousavi *et al.* in explosively welded stainless steel with steel.^[40] The authors explain this morphology by the change of impact angle. It should be noted that our upper interface was of good quality without any pores. Alternatively, the interface located further from the explosive materials (lower interface) was rather planar and no difference in contrast in the backscattered electrons (BSE) imaging mode was found, indicating that chemical homogeneity across the interface was observed (Figure 2(b)). Nevertheless, a few cracks were present within the titanium layer (Figure 2(d)), which did not demonstrate any tendency for further propagation. A waveless interface is typical for welding modes close to the lower boundary of the welding window.^[41] The morphology and shape of the interfaces strongly depend on the initial parameters of the EXW.^[12] According to Shiran *et al.*,^[12] higher explosive forces promote wavy-mode interfaces. Taking that into account, it can be concluded that the middle Ti clad considerably damped the impact force, thereby reducing its power. However, although the force arriving to the lower interface was not strong enough to induce waviness, it was sufficient to form the lower joint with a flat interface. The use of a thicker Ti clad would probably suppress the welding process of the three-layered material and the lower joint would not be formed, or proneness to some delamination could be expected. It should also be noticed that some reports for three-layered setups, such as Al/Cu/Al,^[42] Zr/Ti/steel,^[43,44] and Al/steel/Al,^[45] have shown a wavy mode for both interfaces.

Another important factor that influences the shape of the interface (wavy with or without vortexes or flat) is the distance from the explosive material. This parameter was studied for multilayered Ti/Al clads in the works of Bataev *et al.*,^[24] Pavliukova *et al.*,^[33] and Lazurenko *et al.*,^[25] or for sandwiches of low-carbon steel setups in works of Bataev *et al.*^[46] In all these mentioned works, the examination was focused on the wavy mode of the interface, whereas the chemical composition was only analyzed in the vortex areas in the upper interfaces.

As can be seen in Figure 3, the upper interface region is not uniform in composition and a zone with some particles in the Al clad can be distinguished. Such an effect is shown in the works of Greenberg *et al.*^[47,48] and

is known as granulating fragmentation (GF). GF was observed in both wavy and planar interfaces. It is also observed for other systems, *i.e.*, copper-tantalum or iron-silver.^[48] It can also be noticed in the same figure that the upper interface possesses intermetallic phase-rich areas. However, in contrast to our previous studies, they did not form peninsula- or island like structures.^[30,31] According to the Ti-Al phase equilibrium diagram,^[49] three stable phases, namely, Ti_3Al , $TiAl$, and $TiAl_3$, or a metastable $TiAl_2$ phase, can be formed. The chemical composition analysis carried out

in intensely mixed node regions by means of SEM/EDS revealed the presence of $TiAl_2$, $TiAl$, and $TiAl_3$ phases (examples in the tables in Figure 3). However, the SEM/EDS measurements have to be supported by other analytical techniques, since, as reported in the literature, an accelerating voltage of 12 kV induces an interaction volume of about $1.2 \mu m^3$, which implies that signals coming from different phases might be included.^[30]

Comparison of the upper and lower interfaces confirmed that dissimilar scenarios occurred on each interface, and as a result, different morphologies,

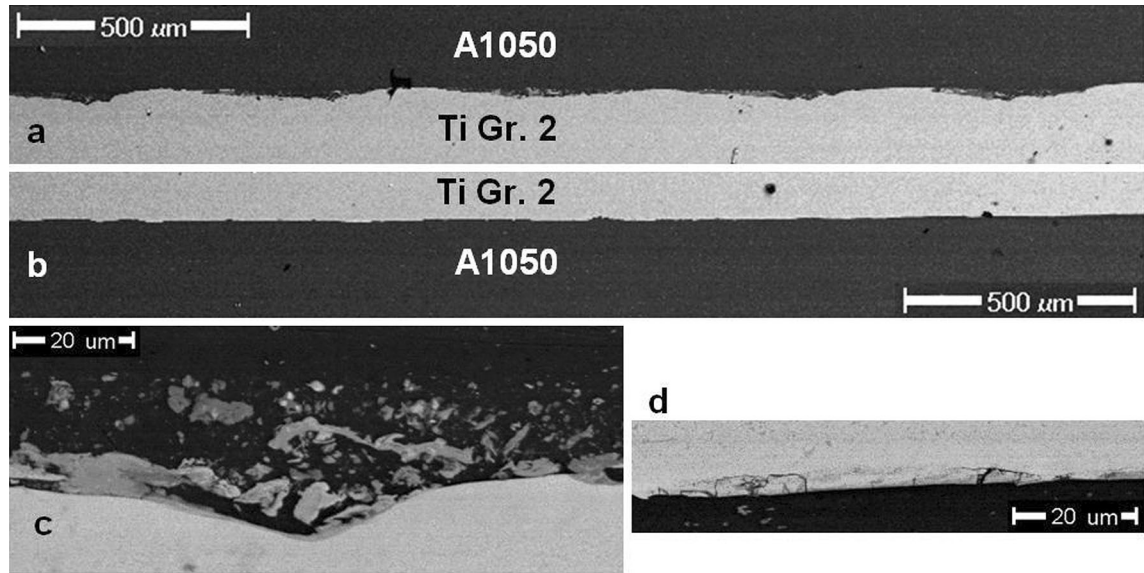


Fig. 2—SEM/BSE images presenting the influence of the collision angle on the interface shape: (a) the wavy mode with (c) swirled intermetallic phases and (b) the flat mode with (d) noticeable cracks within the titanium layer.

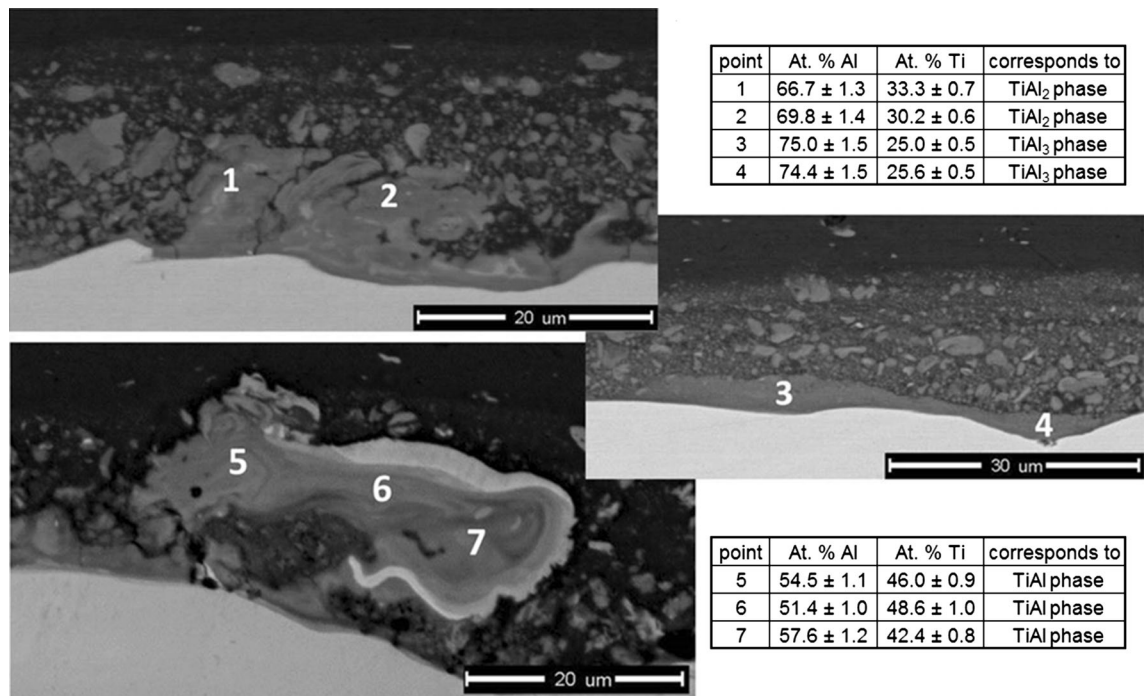


Fig. 3—SEM/BSE micrograph of the upper interface of the clad together with the results of the EDS analysis.

microstructures, and chemical compositions were obtained. As mentioned previously, the upper interface, because of its closer proximity to the explosive material, was exposed to a greater impact force and, as a consequence, apart from the waviness, was characterized by a significantly more complex microstructure with swirled intermetallics, as well as intermediate phases scattered within the Al clad. Evidently, the energy available is used partly to plastically deform the clad, and there is a fraction that is transformed into heat, which promotes the nucleation and growth of other phases. This phenomenon has also been reported in the past,^[12] with an increase in the explosive force being the reason for higher plastic deformation of ingoing materials, correlated with an increase of the intermetallic layer thickness within the 321 austenitic stainless steel/1230 aluminum alloy assembly.

Therefore, each interface represents a different initial condition for the heat treatments and directly affects the

microstructural evolution. It is expected that the intermetallic phase growth will be enhanced on the upper interface, in comparison with the lower one, during the annealing process due to several reasons. According to the observation cited previously, a larger amount of energy should have been stored as deformation in the upper interface upon EXW, in comparison with the lower one. In addition, the energy barrier needed for nucleation should have already been overcome in the former. Furthermore, a stronger grain refinement of the aluminum is observed near the upper interface, which provides more available paths for grain boundary diffusion and, in turn, enhances the growth process. Of course, this also depends strongly on the type of grain boundaries and is only true for high-angle grain boundaries (HAGBs).

For a more detailed characterization, the crystallographic information on the microstructure of the joined metals in the region close to the interfaces was acquired using the EBSD technique. As a result, two EBSD maps, collected for the upper and lower interface regions, are shown in Figure 4. In both Al clads, some wavy alignment of elongated grains was distinguished; however, the wave character is much more pronounced within the upper Al (flyer) plate. A remarkable grain refinement can be observed in areas directly adjacent to the joint. This refined region mainly consisted of Al crystallites and some intermetallics, which upon annealing at high temperature would grow. The shape of the titanium grains is more equiaxed, as can be clearly seen in Figure 4.

The EBSD map revealed a strongly twinned microstructure with a much higher amount of twins and secondary twins close to the upper interface area than observed in the neighborhood of the lower interface. Additionally, from the grain size distribution for Al plotted in Figure 5, it can be clearly seen that in the region shown in the EBSD maps (up to 150 μm from the interface), more small grains were present in the Al upper clad than in the Al lower one (volume fraction of grains smaller than 10 μm equal to 72.3 pct vs 68.4 pct for the upper and lower parts, respectively). This tendency was even more pronounced in the Ti regions, where the upper part contained significantly more twin boundaries (64.6 vs 42.7 pct, respectively). Moreover, the EBSD analysis shows that the average grain sizes for Al are 8.9 and 10.1 μm , while for Ti, they are 9.3 and 12.4 μm , for the upper and lower interface regions, respectively. In general, the refinement of the grains, resulting from large plastic deformation, is more intense in the material located closer to the explosive material; however, this effect is more intense for titanium than for aluminum. This remark is consistent with the observations discussed previously.

Figure 6 shows the grain boundary distribution of aluminum and titanium clads located close to the upper and lower interfaces. Grain boundaries with misorientation angles lower than 5 deg were not taken into consideration. A higher fraction of low-angle grain boundaries (LAGBs, less than 15 deg) was observed for the lower Al region than for the upper one (39.5 pct compared to 36.0 pct, Figures 6(a) and (c)). The same

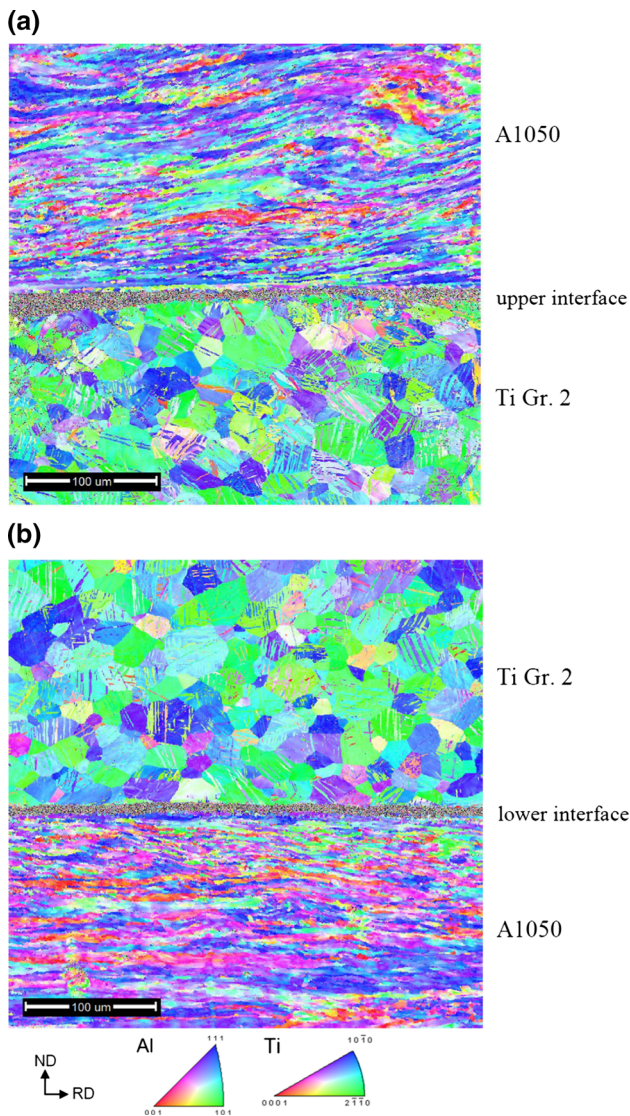


Fig. 4—SEM/EBSD images presenting the microstructure of the (a) upper and (b) lower interfaces of the Al/Ti/Al sample.

tendency was detected for the Ti clad (41.2 to 37.9 pct). This confirms what was stated previously, namely, that a higher number of HAGBs in the upper region promote more intensive growth of the intermetallic layer during annealing because of the enhanced grain boundary diffusion. Additionally, a higher fraction of boundaries can be observed in the misorientation profile at angles of 29 deg and close to 60 deg, indicating a high fraction of HAGBs and twin boundaries, respectively. The twin-type boundaries can be easily ascribed using the Brandon criterion, including peaks close to 55, 58, and 61 deg.

All of these microstructural features strongly suggest that EXW deforms the upper interface of Al and Ti clads more strongly, since more small grains, HAGBs, and twin boundaries were generated close to this interface. It must be stated that the EBSD map of the area located very close to the upper interface (Figure 4(a)) was similar to that obtained in our previous work (Figure 7 in Reference 29), where very fine grains of mostly aluminum and intermetallics were present. The lower interface had a more uniform shape (Figure 4(b)), but again, very fine grains of aluminum and intermetallic phases were observed.

Detailed structural information for the phases present in both interface areas was collected using a monochromatic synchrotron X-ray beam (87.1 keV). By analyzing the diffraction patterns taken from the upper and lower

interfaces, the reflections mainly coming from Al and Ti can be distinguished (Figures 7(a) and (b)). The samples for synchrotron measurements were separated along the titanium clad in order to investigate each interface independently (red dashed lines in Figure 1(b)). Since the two pieces cut from the samples did not have the same thickness of titanium clad, differences in the titanium reflection intensities between Figures 7(a) and (b) existed. Ege *et al.*^[50] reported that flat interfaces are usually more homogenous and contain no intermetallic phases compared to wavy ones, where intermetallics are only present within the molten areas. This occurs due to an adiabatic rise of temperature, which favors the formation of intermetallics. Moreover, Ghaderi *et al.*^[51] concluded that melting or diffusion did not occur at flat interfaces in EXW commercially pure A1100 with AZ31 Mg alloy.

However, a further analysis with a different intensity scale in the middle of the diffraction patterns showed some additional reflections, which were attributed to intermetallic phases. As can be seen, three phases at both interfaces were detected, *i.e.*, Ti₃Al, TiAl, and TiAl₃ (Figures 7(c) and (d)). Additionally, in the upper interface, TiAl₂ was observed (Figure 7(d)). There are other metastable phases that have been found in the literature, such as Ti₃Al₅ and *h*-TiAl₂, as shown by Lazurenko *et al.*^[25] and Palm *et al.*^[52]; however, these were not observed in the current study. As presented in

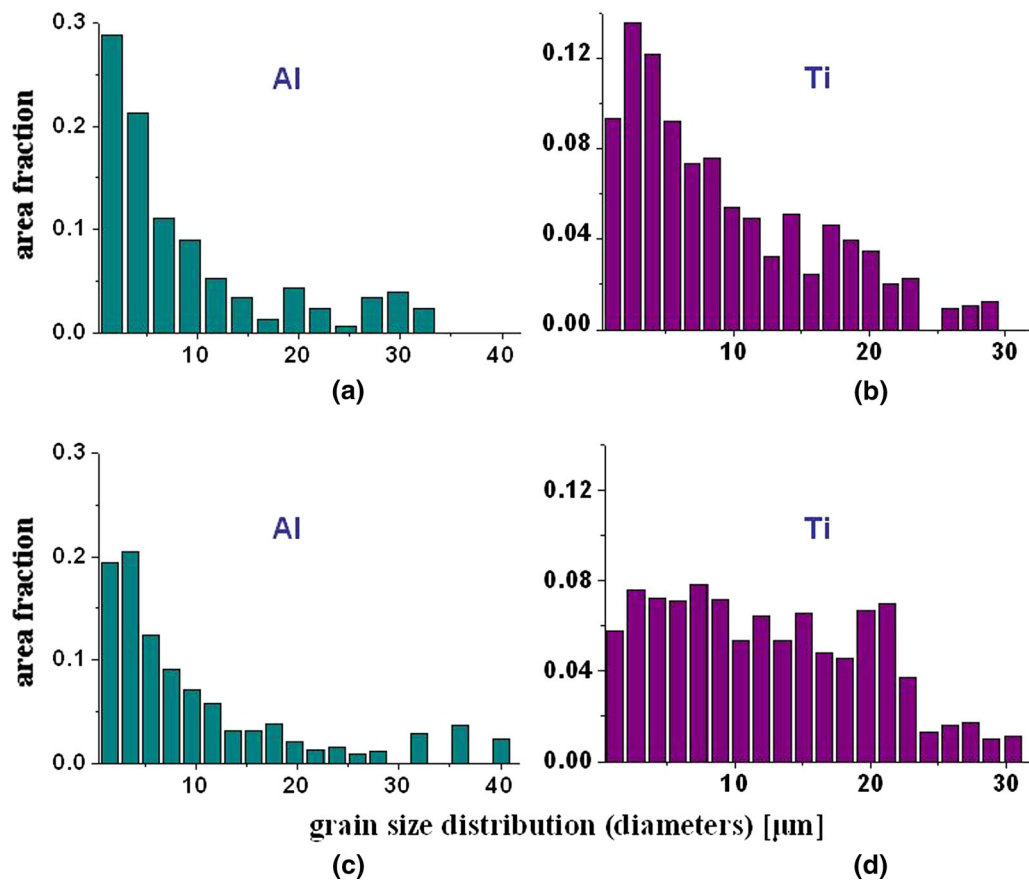


Fig. 5—Histogram of grain size distribution (diameters) calculated from EBSD maps presented in Fig. 4 for the upper ((a) Al and (b) Ti) and lower ((c) Al and (d) Ti) interfaces.

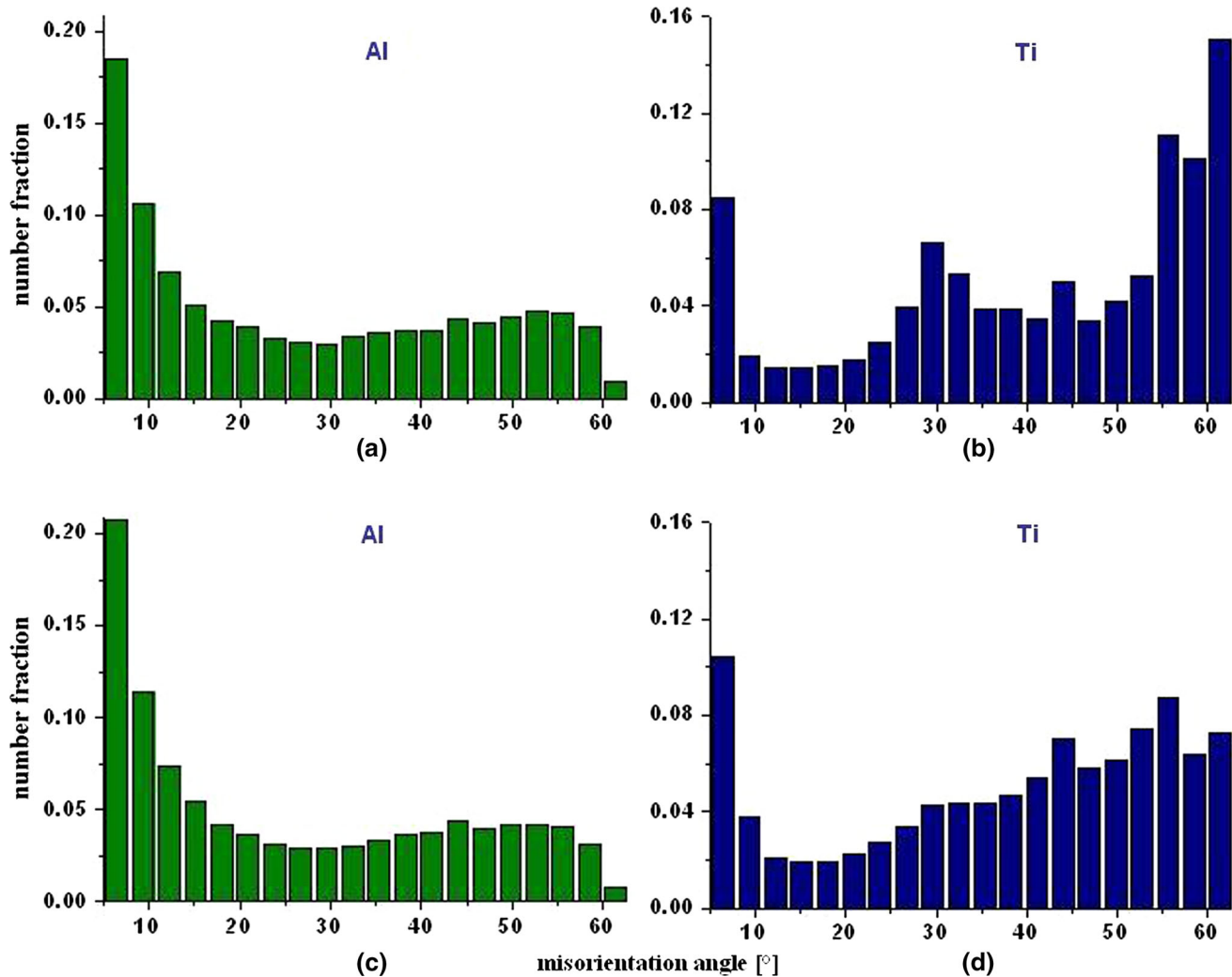


Fig. 6—Misorientation distribution of grain boundaries calculated from EBSD maps presented in Fig. 4 for the upper ((a) Al and (b) Ti) and lower ((c) Al and (d) Ti) interfaces.

our previous work,^[30] a small intensity of the analyzed reflections indicates a minor volume fraction of intermetallics in the sample. Additionally, intermetallic crystallites were not randomly oriented and some degree of texture was present. This was the reason why the approach proposed by Saksl *et al.*^[53] to estimate the volume fraction for each of the phases could not be applied.

B. Heat Treatment

Thermally activated interdiffusion of elemental Ti and Al was observed after annealing for 100 hours at 903 K (630 °C) under a vacuum atmosphere, and the growth of a continuous TiAl₃ intermetallic layer between Al and Ti clads was noticed (Figure 8). Figures 8(b) and (c) show the distribution of Al and Ti, confirming the chemical homogeneity of both layers. For the upper and lower interfaces, the width of the TiAl₃ layer reached 235.3 ± 23.9 and 167.4 ± 19.9 μm , respectively. As expected, the localization of the interfaces in regard to the explosive materials plays a crucial role in

intermetallic occurrence and growth. Hence, enhanced initial conditions for further intermetallic development induced by heat treatment appeared at the upper interface. Two main facts can be mentioned as having been more pronounced at the upper interface after EXW, namely, a thicker area with refined grains and a larger amount of HAGBs, which are direct consequences of more extreme conditions during the process. As commented previously, a larger number of nuclei or places for heterogeneous nucleation (more refined grains) at the upper interface neighborhood may lead to a decrease of the incubation time during the intermetallic phase growth. Of course, these differences will depend on the parameters of the EXW. However, once this time is overcome, the growth rate should be similar for the same phase.

We now compare the results obtained in the current work with those reported in the literature concerning the growth of phases upon annealing. According to the present work, the location within the multilayered composites plays an important role, as different conditions of EXW occur on each interface. Hence, each

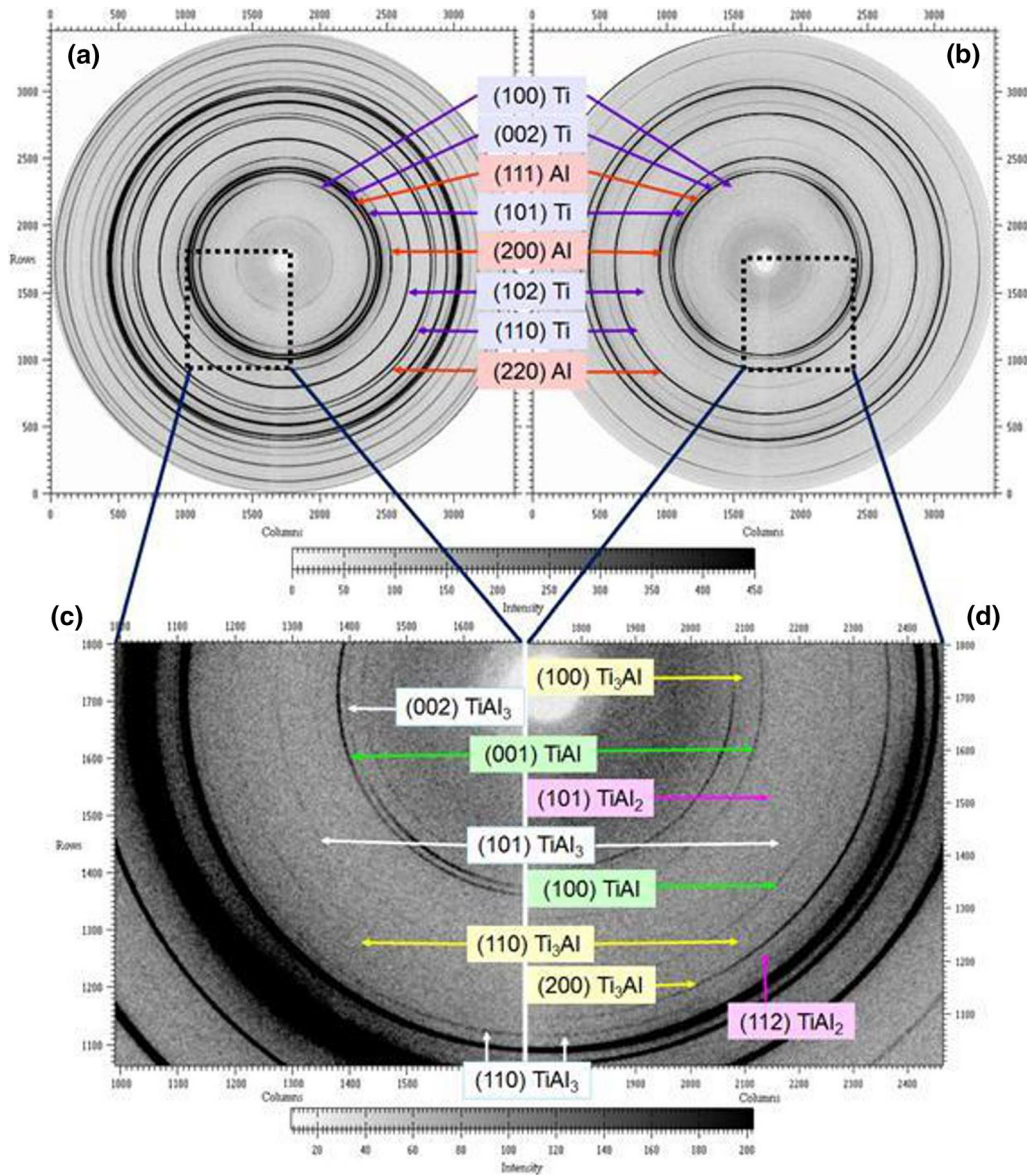


Fig. 7—X-ray synchrotron diffraction of (a) lower and (b) upper interfaces of the Al/Ti/Al sample. (c) and (d) Enlarged central parts of the diffraction patterns with different intensity scale demonstrate the low intensity reflections.

interface should be considered separately, especially when many layers, for example, 6^[32] or 40^[25] are investigated. However, this fact was not clearly emphasized in the works of Foadian *et al.*^[32] and Lazurenko *et al.*^[25] These authors did not indicate which interfaces were taken into consideration for the kinetics calculations. Therefore, it can be presumed that the data were averaged. Moreover, an external load may also have a strong influence on the intermetallic layer growth, meaning calculations for samples with and without compression should be conducted individually for each case, which was not applied in Reference 25. Thus, the examination of the growth kinetics for each interface separately is planned for future works.

In our previous work, the intermetallics layer was $95.7 \pm 9.9 \mu\text{m}$ in width for two-layered Ti/Al samples annealed under the same conditions.^[30] In the current

work, both interfaces were of good quality without pores or hollows, in contrast to the interface in two-layered Ti/Al shown in Figure 5(e) in Reference 31. Both types of clads were manufactured with the use of a detonation velocity in the range of 1900 to 1950 m/s. This confirms that the other initial manufacturing conditions, such as collision angle or detonation pressure, also play a crucial role in determining strongly not only the microstructure of the obtained platter but also the growth velocity of the intermetallic phase at the interface during heat treatment.

Upon annealing, twins are annihilated in Ti during grain growth by twin boundary motion and grain boundary migration. The annealing process also induces a growth of two single crystalline Al layers (Figure 8(a)). Both Al layers possess a random orientation, and no common high index plane or axis between them was

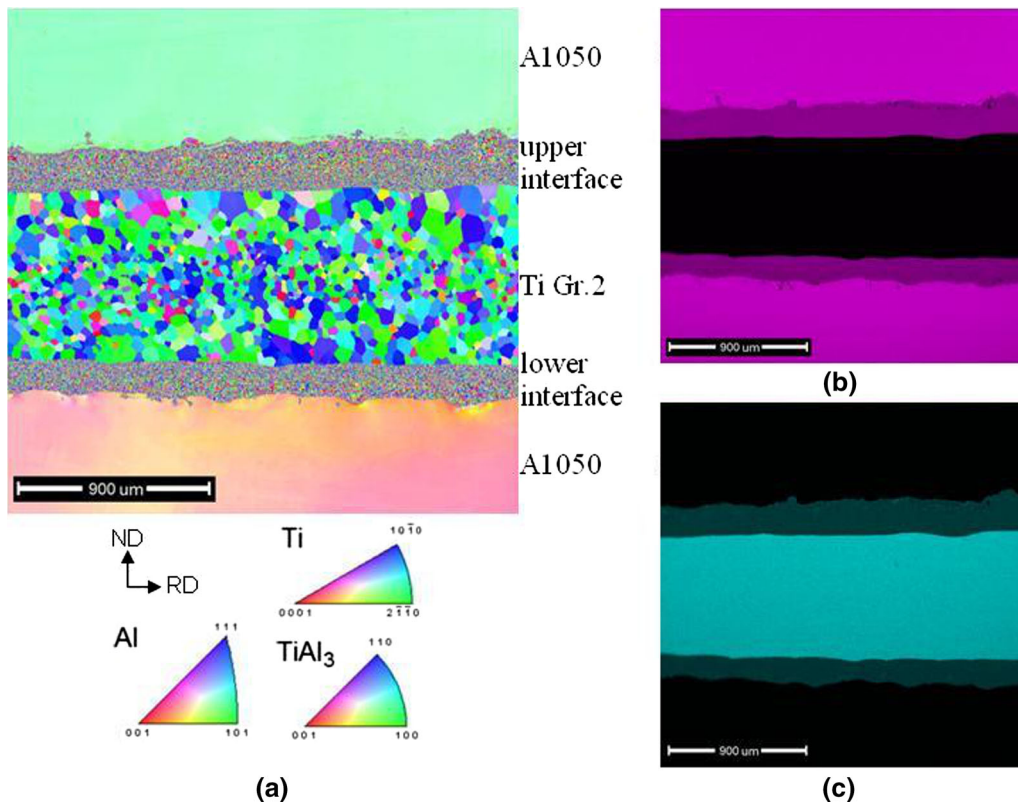


Fig. 8—(a) SEM/EBSD image presenting the microstructure of the upper and lower interfaces of the Al/Ti/Al sample after annealing at 903 K (630 °C) for 100 h in a vacuum and maps showing the distribution of elemental (b) Al and (c) Ti across the sample (a).

found. A single crystalline layer of Al has barely been described in the literature.^[54–56] However, it does not exclude composites containing single crystals from future studies confirming its potential application.

C. Thin Foil Investigation

An electron transparent thin foil was cut from the upper interface, in particular, from the region where intermetallic crystallites were randomly distributed within the refined Al grains. Bright-field (BF) and dark-field (DF) images obtained from this region show many fine grains (up to 600 nm in size, Figures 9(a) and (b)). The electron diffraction pattern confirmed the presence of intermetallic grains randomly distributed within Al (Figure 9(c)). The phase analysis completed by a selected area diffraction pattern (SADP) showed two stable phases, namely, Ti_3Al and $TiAl$, and one metastable phase, $TiAl_2$, while the $TiAl_3$ phase was not detected. The $TiAl_2$ intermetallic phase was also detected in our previous work concerning two-layered Ti/Al samples,^[30,31] although in other works on the Ti/Al system, it was not observed.^[22,24,32–34]

Subsequently, the investigated thin foil was annealed for 1 hour at 825 K (552 °C) in a calorimeter in order to observe the influence of postheating on structural heterogeneity and phase changes. Upon annealing, the lamella microstructure changed significantly and grain growth became more significant (Figure 9(d)). As can be seen in the DF images in Figures 9(b) and (e), the

average grain size changed from about 150 to 220 nm. The SADP analysis revealed only $TiAl_3$ (Figure 9(f)), which is thermodynamically and kinetically most favored.^[57,58] Thus, it can be concluded that the annealing mainly causes $TiAl_3$ growth at the cost of other intermetallic phases, since only this phase was observed after annealing.

D. Vickers Hardness Test

The average hardness values of the parent Al and Ti clads are determined to be 34 and 180 HV, respectively. The Vickers hardness profile measured for the cross section of the Al/Ti/Al sample is presented in Figure 10. The average hardness values for the aluminum base plate, titanium flyer plate, and aluminum flyer plate were 34, 187, and 36 HV, respectively. The component hardness only slightly increased due to the EXW process. Conversely, a significant increase in hardness values for both Cu and Al explosively welded clads was observed in the work of Honarpisheh *et al.*^[42] Cu and Al, as starting materials, had 26 and 54 HV, and after EXW, 50 to 52 HV and 102 to 103 HV, respectively. Mamalis *et al.*^[59] explained the increase in hardness values by the stress waves and the intense thermal impact, which seems not to play a significant role in the current study.

The microstructure in both aluminum clads changed significantly from the typical rolled materials due to the high-speed crash of plates, *i.e.*, plastic deformation. In

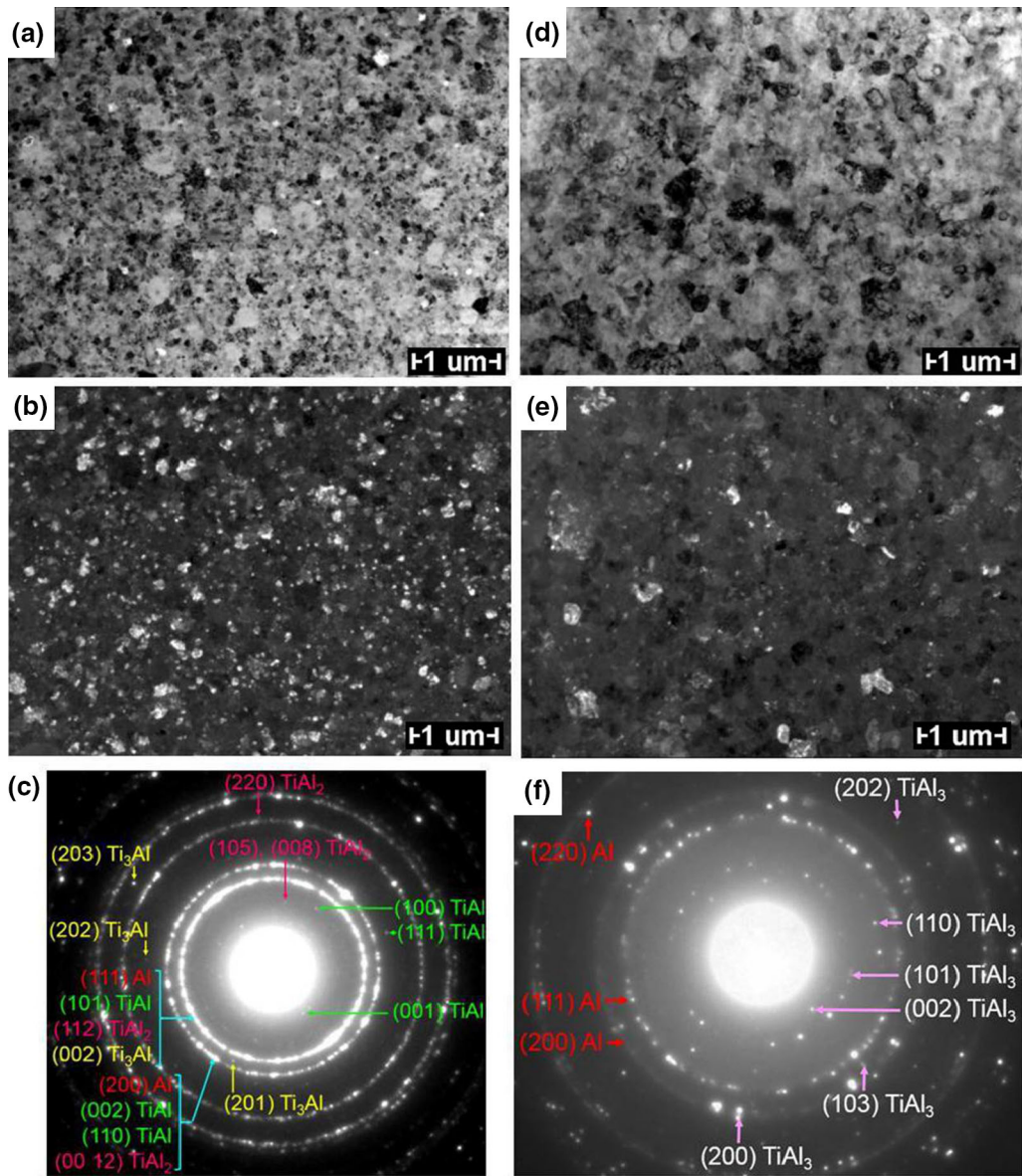


Fig. 9—TEM images of microstructure of the interface area in the state directly after EXW ((a) BF and (b) DF) and annealing ((d) BF and (e) DF) with corresponding SADPs ((c) and (f), respectively).

both plates, the elongated grains caused hardness variation. A decrease of hardness in the area neighboring the interface in the Al flyer plate was detected. The same phenomenon was detected in explosively welded carbon steel/Zr 700 samples in the work of Paul *et al.*^[60] When the hardness measurements were performed within the melted regions, a visible decrease in hardness was detected.

It should be noted that the Ti clad, placed between the Al plates, was characterized by a large scatter of hardness values. The increase occurred due to the presence of deformation twins formed as a result of plastic deformation after the intense shock. The lower hardness values can be correlated to areas without twins. Consequently, the strength of the obtained Ti clad is larger than that for the rolled one.^[61] As can be seen in Figure 10, all indentations were square shaped

without separation or cracks around edges or diagonals. The intermetallic regions were too small for the Vickers hardness measurements.

IV. SUMMARY AND CONCLUSIONS

The aim of the current work was to relate the microstructure and phase composition changes with the localization of the interface regarding the explosive material placement. The simpler case of two interfaces (Al/Ti/Al) joined by EXW was examined. The effect of subsequent annealing was also studied. A comprehensive examination revealed significant differences between the two interfaces (upper and lower), with the following conclusions.

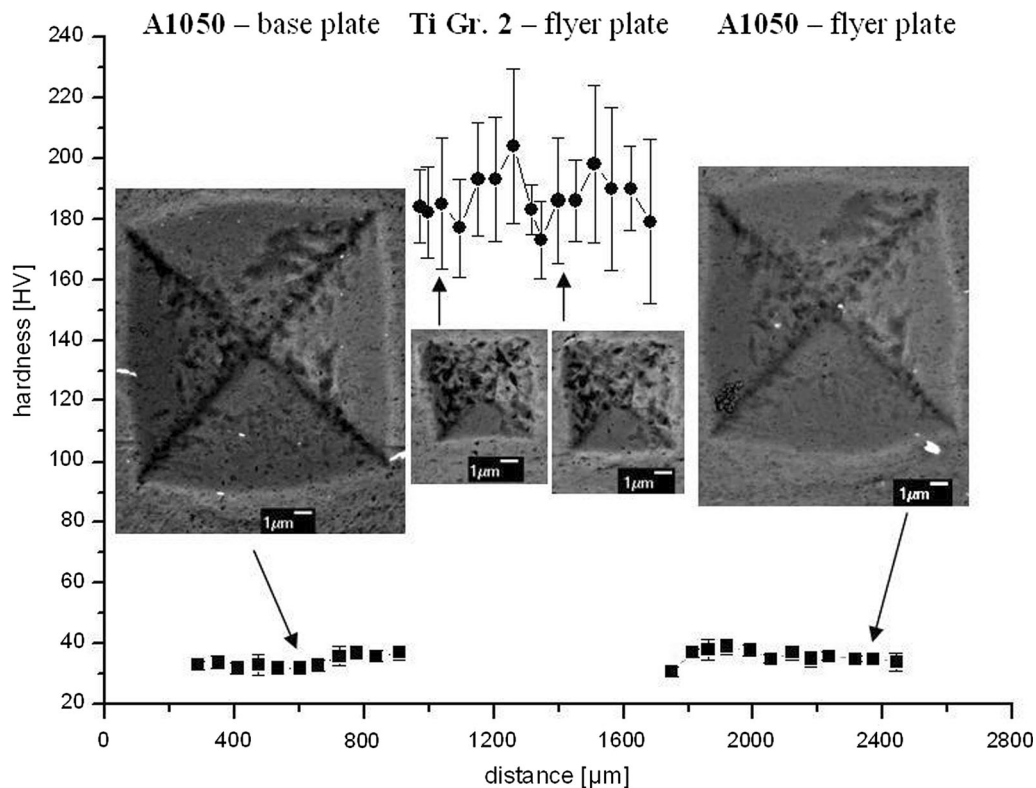


Fig. 10—Vickers hardness profile through the Al/Ti/Al sample with the SEM images of the indentations.

1. Al possesses a slightly finer microstructure in the area closer to the upper interface than the lower interface. The same tendency, but more pronounced, was obtained for titanium. Additionally, a more intense plastic deformation caused a higher number of HAGBs and twin boundaries in the Ti clad, in the area adjacent to the upper interface.
2. A higher fraction of LAGBs in the Al clad was found in the region close to the lower interface, and the same tendency was obtained in Ti. Additionally, more HAGBs with misorientation of about 29 deg, twinning, and secondary twinning were observed in the upper interface in Ti.
3. Considerable differences in morphology and the chemical composition between upper and lower interfaces appeared in the state directly after EXW. The three intermetallic phases, Ti_3Al , $TiAl$, and $TiAl_3$, were detected at both interfaces using TEM and synchrotron diffraction, while the metastable $TiAl_2$ was only detected in the upper interface. The fraction of intermetallics in the entire system is minimal. If we compare the zones corresponding to the upper and lower interfaces, the amount of intermetallics is higher at the interface close to the explosive material, exhibiting no regularity in their distribution.
4. An ulterior annealing treatment performed at 903 K (630 °C) for 100 hours in a vacuum allowed receiving single crystal of Al in the obtained Al/ $TiAl_3$ /Ti/ $TiAl_3$ /Al system. Furthermore, the interfaces had similar chemical composition after heat

treatment composed of mainly the $TiAl_3$ phase; however, an enormous difference for the continuous intermetallic layer thickness was measured, reaching values of 235.3 and 167.4 μm for upper and lower interfaces, respectively.

5. Vickers hardness measurements did not reveal significant differences related to the localization of the hardness measurements for the upper and lower plates of aluminum. A large scatter of hardness values obtained for Ti was attributed to the presence of deformation twins formed due to plastic deformation during the EXW process.

ACKNOWLEDGMENTS

The authors thank High Energy Technologies Works 'Explomet' (Opole, Poland) for the provision of the good quality Al/Ti/Al clads. Samples were examined in the Accredited Testing Laboratories, Institute of Metallurgy and Materials Science, Polish Academy of Sciences (Krakow). Part of the SEM observations were performed in the frame of the Erasmus+ programme.

CONFLICT OF INTEREST

The authors declare that they have no conflict of interest.

OPEN ACCESS

This article is distributed under the terms of the Creative Commons Attribution 4.0 International License (<http://creativecommons.org/licenses/by/4.0/>), which permits unrestricted use, distribution, and reproduction in any medium, provided you give appropriate credit to the original author(s) and the source, provide a link to the Creative Commons license, and indicate if changes were made.

REFERENCES

1. T.Z. Blazynski: *Explosive Welding, Forming and Compaction*, Springer, Dordrecht, 1983.
2. A.R. Farinha, R. Mendes, J. Baranda, R. Calinas, and M.T. Vieira: *J. Alloys Compd.*, 2009, vol. 483, pp. 235–38.
3. J. Bystrzycki, J. Paszula, R. Trebinski, and R.A. Varin: *J. Mater. Sci.*, 1994, vol. 29, pp. 6221–26.
4. D.J. Mynors and B. Zhang: *J. Mater. Process. Technol.*, 2002, vol. 125, pp. 1–25.
5. H. Mehrasa, G. Liaghat, and D. Javabvar: *Cent. Eur. J. Eng.*, 2012, vol. 2, pp. 656–64.
6. H. Paul, L. Litynska-Dobrzynska, and M. Prazmowski: *Metall. Mater. Trans. A*, 2013, vol. 44A, pp. 3836–51.
7. M. Acarer, B. Gulenc, and F. Findik: *J. Mater. Sci.*, 2004, vol. 39, pp. 6457–66.
8. Y. Aizawa, J. Nishiwaki, Y. Harada, S. Muraishi, and S. Kumai: *J. Manuf. Proc.*, 2016, vol. 24, pp. 100–06.
9. Q. Chu, M. Zhang, J. Lia, and C. Ya: *Mater. Sci. Eng. A*, 2017, vol. 689, pp. 323–31.
10. G. Xunzhong, T. Jie, W. Wentao, L. Huaguan, and W. Chen: *Mater. Des.*, 2013, vol. 49, pp. 116–22.
11. E. Zamani and G.H. Liaghat: *J. Mater. Sci.*, 2012, vol. 47, pp. 685–95.
12. M.R.K.G. Shiran, H. Bakhtiari, S.A.A.A. Mousavi, G. Khalaj, and S.M. Mirhashemi: *Mater. Res.*
13. W. Sun, X. Li, H. Yan, and K. Hokamoto: *J. Mater. Eng. Perform.*, 2014, vol. 23, pp. 421–28.
14. M.A. Habib, H. Keno, R. Uchida, A. Mori, and K. Hokamoto: *J. Mater. Process. Technol.*, 2015, vol. 217, pp. 310–16.
15. K. Hokamoto, K. Nakata, A. Mori, S. Tsuda, T. Tsumura, and A. Inoue: *J. Alloys Compd.*, 2009, vol. 472, pp. 507–11.
16. S. Narayan, S. Tanaka, A. Mori, and K. Hokamoto: *J. Mater. Process. Technol.*, 2017, vol. 245, pp. 300–08.
17. R. Chulist, D.M. Fronczek, Z. Szulc, and J. Wojewoda-Budka: *Mater. Charact.*, 2017, vol. 129, pp. 242–46.
18. J.H. Han, J.P. Ahn, and M.C. Shin: *J. Mater. Sci.*, 2003, vol. 38, pp. 13–18.
19. B. Gulenc, Y. Kaya, A. Durgutlu, I.T. Gulenc, M.S. Yildirim, and N. Kahraman: *Arch. C Mech. Eng.*, 2016, vol. 16, pp. 1–8.
20. H.R. Pakzaman, M. Divandari, and A.R. Khavandi: *IIAC2012, Arak, I.R. Iran*, 2012, May, pp. 1–7.
21. P. Wang, J. Chen, Q. Li, D. Liu, P. Huang, F. Jin, Y. Zhou, and B. Yang: *Fus. Eng. Des.*, 2017.
22. H. Xia, S. Wang, and H. Ben: *Mater. Des.*, 2014, vol. 56, pp. 1014–19.
23. P. Bazarnik, B. Adamczyk-Cieslak, A. Galka, B. Plonka, L. Sniezek, M. Cantonie, and M. Lewandowska: *Mater. Des.*, 2016, vol. 111, pp. 146–57.
24. I.A. Bataev, A.A. Bataev, V.I. Mali, and D.V. Pavliukova: *Mater. Des.*, 2012, vol. 35, pp. 225–34.
25. D.V. Lazurenko, I.A. Bataev, V.I. Mali, A.A. Bataev, I.N. Maliutina, V.S. Lozhkin, M.A. Esikov, and A.M.J. Jorge: *Mater. Des.*, 2016, vol. 102, pp. 123–30.
26. K.S. Vecchio: *JOM*, 2005, vol. 57, pp. 25–31.
27. M.M. Hoseini Athar and B. Tolaminejad: *Mater. Des.*, 2015, vol. 86, pp. 516–25.
28. P. Chen, J. Feng, Q. Zhou, E. An, J. Li, Y. Yuan, and S. Ou: *J. Mater. Eng. Perform.*, 2016, vol. 25, pp. 2635–41.
29. B. Wang, F. Xie, B. Wang, and X. Luo: *Mater. Sci. Eng. C*, 2015, vol. 50, pp. 324–31.
30. D.M. Fronczek, J. Wojewoda-Budka, R. Chulist, A. Sypien, A. Korneva, Z. Szulc, N. Schell, and P. Zieba: *Mater. Des.*, 2016, vol. 91, pp. 80–89.
31. D.M. Fronczek, R. Chulist, L. Litynska-Dobrzynska, Z. Szulc, P. Zieba, and J. Wojewoda-Budka: *J. Mater. Eng. Perform.*, 2016, vol. 25, pp. 3211–17.
32. F. Foadian, M. Soltanieh, M. Adeli, and M. Etminanbakhsh: *Metall. Mater. Trans. A*, 2014, vol. 45A, pp. 1823–32.
33. D.V. Pavliukova, V.I. Mali, A.A. Bataev, P.S. Yartsev, T.S. Sameyshcheva, and L.I. Shevtsova: *8th IFOST*, 2013, pp. 183–86.
34. N. Kahraman, B. Gulenc, and F. Findik: *Int. J. Impact Eng*, 2007, vol. 34, pp. 1423–32.
35. K. Hokamoto, Y. Ujimoto, and M. Fujita: *Mater. Trans.*, 2004, vol. 45, pp. 2897–2901.
36. J.R. Feng, P.W. Chen, K.D. Dai, E.F. An, and Y. Yuan: *Mater. Sci. Forum*, 2014, vol. 767, pp. 114–19.
37. R. Mendes, J.B. Ribeiro, and A. Loureiro: *Mater. Des.*, 2013, vol. 51, pp. 182–92.
38. G. Rogalski, D. Fydrych, and W. Walczak: *Przegląd Spawalnictwa*, 2013, vol. 6, pp. 54–59 (in Polish).
39. K. Hokamoto, A. Chiba, M. Fujita, and T. Izuma: *Compos. Eng.*, 1995, vol. 5, pp. 1069–79.
40. A.A. Akbari Mousavi and S.T.S. Al-Hassani: *J. Mech. Phys. Solids*, 2005, vol. 53, pp. 2501–28.
41. A.A. Berdychenko, L.B. Pervukhin, and O.L. Pervukhina: *Met. Sci. Heat Treat.*, 2009, vol. 51, pp. 476–81.
42. M. Honarpisheh, M. Asemabadi, and M. Sedighi: *Mater. Des.*, 2012, vol. 37, pp. 122–27.
43. M.J. Duan, Y. Wang, J. Hong, J. Zhou, and R. Ma: *Adv. Mater. Res.*, 2014, vols. 926–930, pp. 354–57.
44. J. Ning, L. Zhang, M. Xie, H. Yang, X. Yin, and J. Zhang: *J. Alloys Compd.*, 2017, vol. 698, pp. 835–51.
45. M. Honarpisheh, J. Niksokhan, and F. Nazari: *Metall. Res. Technol.*, 2016, vol. 113, p. 105.
46. I.A. Bataev, A.A. Bataev, V.I. Mali, V. Burov, E. Golovin, A. Smirnov, and E. Prikhodko: *Adv. Mater. Res.*, 2011, vol. 287, pp. 108–11.
47. B.A. Greenberg, M.A. Ivanov, A.V. Inozemtsev, A.M. Patselov, M.S. Pushkin, and A.M. Vlasova: *Metall. Mater. Trans. A*, 2015, vol. 46A, pp. 3569–80.
48. B.A. Greenberg, M.A. Ivanov, V.V. Rybin, O.A. Elkina, O.V. Antonova, A.M. Patselov, A.V. Inozemtsev, A.V. Plotnikov, A.Y. Volkova, and Y.P. Beshshaposhnikov: *Mater. Charact.*, 2013, vol. 75, pp. 51–62.
49. H. Okamoto: *Binary Alloy Phase Diagrams Updating Service*, ASM International, Materials Park, OH, 1992.
50. E.S. Ege, O.T. Inal, and C.A. Zimmerly: *J. Mater. Sci.*, 1998, vol. 33, pp. 5327–38.
51. S.H. Ghaderi, A. Mori, and K. Hokamoto: *Mater. Trans.*, 2008, vol. 5, pp. 1142–47.
52. M. Palm, N. Engberding, F. Stein, K. Kelm, and S. Irsen: *Acta Mater.*, 2012, vol. 60, pp. 3559–69.
53. K. Saksil, D. Ostrushko, E. Mazancova, Z. Szulc, O. Milkovic, M. Durisin, D. Balaga, J. Durisin, U. Rutt, and O. Gutowski: *Int. J. Mater. Res.*, 2015, vol. 106, pp. 621–27.
54. H. Huang and J.R. Asay: *J. Appl. Phys.*, 2007, vol. 101, p. 063550.
55. A.S. Khan, J. Liu, J.W. Yoon, and R. Nambori: *Int. J. Plast*, 2015, vol. 67, pp. 39–52.
56. M. Gautier, E. Marteaux, J.P. Duraud, R. Baptist, A. Brenac, and D. Spanjaar: *J. Vac. Sci. Technol. A*, 1987, vol. 5, pp. 50–54.
57. Y. Wei, W. Aiping, Z. Guisheng, and R. Jialie: *Mater. Sci. Eng., A*, 2008, vol. 480, pp. 456–63.
58. L. Xu, Y.Y. Cui, Y.L. Hao, and R. Yang: *Mater. Sci. Eng. A*, 2006, vol. 435, pp. 638–47.
59. A.G. Mamalis, N.M. Vaxevanidis, A. Szalay, and J. Prohaszka: *J. Mater. Process. Technol.*, 1994, vol. 44, pp. 99–117.
60. H. Paul, J. Morgiel, M. Faryna, M. Prazmowski, and M. Miszczyk: *Int. J. Mater. Res.*, 2015, vol. 106, pp. 782–92.
61. X. Chun and Z. Wen-feng: *Trans. Nonferrous Met. Soc. China*, 2012, vol. 22, pp. 1939–46.